









ARTICLE

<https://doi.org/10.1038/s41467-019-11868-5>

OPEN

Molecular cobalt corrole complex for the heterogeneous electrocatalytic reduction of carbon dioxide

Sabrina Gonglach^{1,8}, Shounik Paul^{2,3,8}, Michael Haas¹, Felix Pillwein ¹, Sreekumar S. Sreejith ^{2,3}, Soumitra Barman^{2,3}, Ratnadip De ^{2,3}, Stefan Müllegger ⁴, Philipp Gerschel⁵, Ulf-Peter Apfel^{5,6}, Halime Coskun⁷, Abdalaziz Aljabour ⁷, Philipp Stadler ⁷, Wolfgang Schöfberger ¹ & Soumyajit Roy ^{2,3}

Electrochemical conversion of CO₂ to alcohols is one of the most challenging methods of conversion and storage of electrical energy in the form of high-energy fuels. The challenge lies in the catalyst design to enable its real-life implementation. Herein, we demonstrate the synthesis and characterization of a cobalt(III) triphenylphosphine corrole complex, which contains three polyethylene glycol residues attached at the *meso*-phenyl groups. Electron-donation and therefore reduction of the cobalt from cobalt(III) to cobalt(I) is accompanied by removal of the axial ligand, thus resulting in a square-planar cobalt(I) complex. The cobalt(I) as an electron-rich supernucleophilic d⁸-configured metal centre, where two electrons occupy and fill up the antibonding d_{z²} orbital. This orbital possesses high affinity towards electrophiles, allowing for such electronically configured metals reactions with carbon dioxide. Herein, we report the potential dependent heterogeneous electroreduction of CO₂ to ethanol or methanol of an immobilized cobalt A₃-corrole catalyst system. In moderately acidic aqueous medium (pH = 6.0), the cobalt corrole modified carbon paper electrode exhibits a Faradaic Efficiency (FE%) of 48 % towards ethanol production.

¹Institute of Organic Chemistry, Johannes Kepler University Linz, Altenberger Straße 69, 4040 Linz, Austria. ²Eco-Friendly Applied Materials Laboratory (EFAML), Materials Science Centre, Department of Chemical Sciences, Mohanpur Campus, Indian Institute of Science Education and Research, Kolkata 741246 West Bengal, India. ³Eco-Friendly Applied Materials Laboratory (EFAML), College of Chemistry, Central China Normal University, 152 Luoyu Road, Wuhan 430079 Hubei, P. R. China. ⁴Institute of Semiconductor and Solid State Physics, Johannes Kepler University Linz, Altenberger Straße 69, 4040 Linz, Austria. ⁵Inorganic Chemistry I, Ruhr-Universität Bochum NC 3/74, Universitätsstraße 150, D-44801 Bochum, Germany. ⁶Fraunhofer UMSICHT, Osterfelder Straße 3, 46047 Oberhausen, Germany. ⁷Institute of Physical Chemistry and Linz Institute of Organic Solar Cells, Johannes Kepler University Linz, Altenberger Straße 69, 4040 Linz, Austria. ⁸These authors contributed equally: Sabrina Gonglach, Shounik Paul. Correspondence and requests for materials should be addressed to W.S. (email: wolfgang.schoefberger@jku.at) or to S.R. (email: s.roy@iiserkol.ac.in)

Minimizing of the CO₂ concentration in the atmosphere is one of the most important challenges in our time^{1,2}. Therefore, the electrochemical reduction of CO₂ to value added chemicals is a sustainable strategy to solve the growing energy crisis, which at the same time has the potential to mitigate environmental pollution. In the past years, the electrochemical reduction of CO₂ has been studied by several research groups to produce valuable products, for example carbon monoxide, formic acid, methane, ethanol, or methanol^{3–5}. Particularly the transformation of CO₂ in high-density alcohols, especially methanol and ethanol, is a cherished goal for chemists and environmental engineers alike^{6,7}. Such transformation of CO₂ to alcohols coupled with the oxidation of water to oxygen⁸ is a promising strategy⁹. However, the low reactivity of carbon dioxide in water with its large energy barrier ($\Delta E = -1366.8$ kJ mol⁻¹)¹⁰ and the competing hydrogen evolution reaction, impedes such transformation, which makes the development of catalysts for electrocatalytic CO₂ reduction to ethanol in aqueous environment a big challenge^{1,2,10}. The thermodynamic reduction potential for CO₂ to methanol and ethanol is 0.03 and 0.09 V (vs. RHE), respectively which is kinetically disfavored. Hence, often CO₂ reducing catalysts end up accruing lot of energy to be operational at a higher potential. In this regard the use of a molecular catalyst with earth abundant elements, (Fe, Mn, Co, Cu, and Ni), especially with a cobalt metal center^{11,12} is a viable alternative as it offers a high degree of tunability with product selectivity at a low overpotential. As early as in 1980s chemists have been successful in reducing CO₂ to CO via electrochemical methods employing catalysts containing different metals like Co¹³, Ni¹⁴, Re^{15–17}, etc. Recently electrochemical reduction of CO₂ to ethanol has been studied in various ways^{18,19}, by tuning the applied potential²⁰, pH²¹, and nature of the electrolyte²² with an aim to control the product selectivity and increase the Faradaic efficiency (FE) as well as to understand the underlying mechanistic pathways. Metal surfaces^{23,24}, oxides²⁵, and alloys^{26,27} are the most explored examples which show good FE for CO₂ reduction but lack selectivity^{28,29} and work at higher overpotentials, involving complex synthetic procedures^{30,31}. Emergent materials like B and N co-doped nanodiamonds exhibit excellent FE (93 %) and selectivity for conversion to ethanol, but work at higher overpotentials¹⁰. Moreover such heteroatom-doped materials³² often require a sophisticated synthetic procedure like chemical vapor deposition, making it hard for large scale implementation³³. We now compare and contrast state of the art catalysts for CO₂ electro-reduction to ethanol, all of which work at higher overpotentials with shorter activity time and have lower FE as compared to the catalyst reported here (Supplementary Table 1). For instance, Cu(100) works at -0.97 V vs. RHE yielding ethanol with a FE% of 14.7²⁹. Further, use of Cu based nano-particles in an ensemble fashion (trans-CuEn) showed a FE% of ethanol formation to be 17 at -0.86 V vs. RHE³⁴. While, with tailoring of cubic Cu nanocrystals to an edge length of 44 nm, FE% of 80 was achieved for CO₂ reduction but the FE% for Ethanol formation was as low as 3.7³⁵. On the other hand, alloys like Cu_xZn show that both the selectivity and FE% of ethanol formation can be governed by tuning the Cu:Zn ratio in the catalyst with a maximum FE% of ethanol formation 29.1 and current density (-3.8 mA cm⁻²) obtained for Cu₄Zn at -1.05 V vs. RHE³⁶. Similarly, electrodeposited Cu–Ag alloy films (6% Ag) exhibit a FE% of ethanol formation to be 25 at -0.7 V vs. RHE with a relatively high current density of -300 mA cm⁻²³⁷. Ethanol was also obtained by tuning the layer thickness of Cu(I)oxide catalysts with a FE% of 9–16 (current density -35 mA cm⁻²) at -0.99 V vs. RHE³⁸, while Cu₂O derived Cu films exhibit FE% of 11.8 at -0.88 V vs. RHE with a current density of -31.2 mA cm⁻²³⁹. Materials like nanodiamonds on B

and N co-doping shows a very good FE% of 93 and selectivity toward ethanol¹⁰.

With the aim to synthesize effective and stable electrocatalysts for CO₂ reduction for the selective ethanol formation, we focus on a molecular Co-corrole catalyst. Metal corroles are structural similar to metal porphyrins with both the metal centers and ligands participating in multielectron redox processes and are promising candidates for efficient proton-coupled electron transfer^{40–42}. These metal complexes stabilize radical intermediates thus providing an effective pathway to facilitate C–C step-up^{43,44}. Cobalt and iron corroles have been previously found to be catalytically active for CO₂ reduction to CO¹².

We thus explore this class of catalysts for CO₂ electroreduction by using cobalt triphenylphosphine 5,10,15-tris(2,3,5,6-tetrafluoro-4-(MeO-PEG(7)thiophenyl) corrole Co(PPh₃) (TpFPC) (-S-PEG(7)-OMe)₃ (“Co-corrole”) where all the three pentafluorophenyl-groups on the *meso*-positions 5, 10, 15 are modified at the *para*-positions by thiol bound PEG(7)-OMe moieties^{45–47}. In the present work, we demonstrate the reduction of CO₂ to alcohols, formaldehyde, carboxylates, and hydrogen with a Co-corrole modified carbon paper electrode working at a low overpotential (-0.8 V vs. RHE) and show the long-term activity of Co-corrole modified carbon paper electrodes, making it as robust as metallic copper electrocatalysts. The molecular cobalt (III)-corrole catalyst is a significant improvement in the matter of selective reduction of CO₂ to value added chemicals.

Results

Synthesis and electrochemical characterization of the catalyst.

The Co-corrole was synthesized via four steps, where the first two steps leading to 5,10,15-tris(pentafluorophenyl)corrole, were performed according to Gryko’s procedure⁴⁸. The electron-withdrawing properties of the C₆F₅ functionalities render the corrole ring electron deficient⁴⁹. Chemical modification with the -S-PEG(7)-OMe moieties at the three *para*-positions of the *meso*-C₆F₅ groups was performed (Fig. 1a) to optimize anchoring and equal distribution of the catalyst on the electrode surface. The chemical syntheses and characterizations are described in detail in the methods section and in the Supplementary Information file (Supplementary Figs. 1–6). The immobilization process of Co-corrole over carbon paper is implemented via drop casting by using acetonitrile solution of Co-corrole. The modified carbon paper electrodes are stable in aqueous solution due to the insolubility of the Co-corrole moiety in water resulting in the formation of a sustainable heterogenized catalyst with extended lifetime for electrocatalysis.

Electrochemical properties of the Co-corrole were investigated by cyclic voltammetry, with glassy carbon as working electrode in CH₃CN under Argon and 0.1 M TBAPF₆ as supporting electrolyte. As shown in Fig. 1b, red curve, two one electron redox peaks at -0.5 V (Co(III)/Co(II)) and -1.5 V (Co(II)/Co(I)) vs. NHE are occurring (Supplementary Fig. 7). The irreversibility of the redox peak at -0.5 V is likely due to the partial loss of the PPh₃ ligand⁵⁰. In analogy to previous report by Kadish et al.⁵⁰, these two couples Co(III)/Co(II) and Co(II)/Co(I) are metal centered redox processes. The reversible two one electron redox peaks at 0.73 and 1.12 V vs. NHE are ligand centered oxidations and correspond to the formation of a cationic and dicationic cobalt(III) corrole complex⁵⁰. DFT calculations suggest that the one-step and the two-step reduction at -0.5 and -1.5 V of the cobalt(III)-corrole leads to enhanced π -back bonding which strengthens the Co–N bonds and the cobalt corrole macrocycle becomes planar (Fig. 1c). Therefore, demetallation is energetically disfavored, which enables catalysis at a single Co(I)-site. The cyclic voltammetry of Co-corrole under CO₂ (Fig. 1b, black

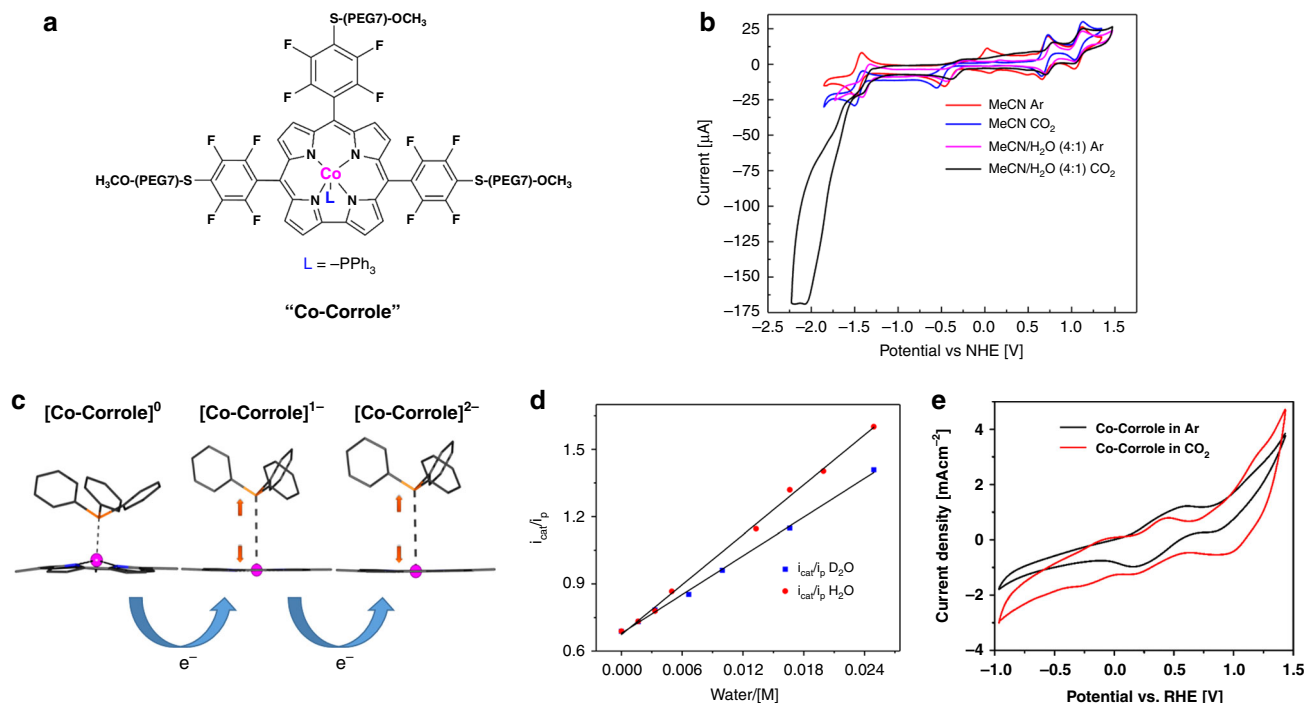


Fig. 1 **a** Chemical structure of the Co-corrole. **b** Cyclic voltammety of Co-corrole dissolved in CH_3CN under Ar (red). Two metal centered redox peaks at -0.5 V (Co (III)/Co(II)) and -1.5 V (Co(II)/Co(I)) vs. NHE could be identified. The irreversibility of the redox peak at -0.5 V is likely due to the partial loss of the PPh_3 ligand. Cyclic voltammety of Co-corrole dissolved in CH_3CN under CO_2 (blue), in $\text{CH}_3\text{CN}/\text{H}_2\text{O}$ (4:1) under Ar (pink) and in $\text{CH}_3\text{CN}/\text{H}_2\text{O}$ (4:1) under CO_2 (black). **c** DFT optimized geometries of $[\text{Co-corrole}]^0$, $1e^-$ and $2e^-$ reduced species showing the movement of Co center into the central cavity of the corrole ring with concomitant lengthening of the Co- PPh_3 bond upon successive reduction. **d** Kinetic isotopic effect demonstrated by cyclic voltammety of Co-Corrole (0.5 mM) recorded in CO_2 saturated in acetonitrile in the presence of varying amount of H_2O or D_2O . Linear dependence of i_{cat}/i_p on the concentration of water (analogous to plotting $\sqrt{k_{\text{CO}_2\text{H}}}$ vs. $[\text{water}]$), $\text{KIE} = k_{\text{CO}_2\text{H}}/k_{\text{CO}_2\text{D}} = (\text{Slope}_{\text{H}_2\text{O}}/\text{Slope}_{\text{D}_2\text{O}})^2 = (37.1057/28.7545)^2 = 1.67$. All cyclic voltammograms were recorded with 0.1 M TBAPF₆ as supporting electrolyte using a glassy carbon as working electrode and a Ag/AgCl as reference electrode at a scan rate of 100 mV s^{-1} . **e** Heterogeneous catalysis of 1 mM Co-corrole on carbon-fiber electrode under Ar (black) and CO_2 (red) at $\text{pH} = 6.0$ (Ag/AgCl/KCl, Pt, 0.1 M NaClO_4 , 100 mV s^{-1})

curve) dissolved in $\text{CH}_3\text{CN}/\text{H}_2\text{O}$ (4:1) shows compared with Co-corrole in ACN under CO_2 (Fig. 1b, blue curve) a steep increase in current at -1.5 V vs. NHE, which confirms that CO_2 reduction occurs in presence of a proton source. A value for the kinetic isotopic effect $\text{KIE} = 1.64$ was determined from the linear plots of i_{cat}/i_p against $[\text{H}_2\text{O}]$ or $[\text{D}_2\text{O}]$ measured at 100 mV s^{-1} (Fig. 1d).

Cyclic voltammety of the Co-corrole modified carbon-fiber electrode under Ar (Fig. 1e, black curve) and CO_2 (Fig. 1e, red curve) was investigated in aqueous conditions at $\text{pH} = 6.0, 7.2,$ and 8.0 (Supplementary Figs. 8–14, Co-corrole physisorbed on carbon paper). In all cases, a steep increase in catalytic current could be detected at a potential of -0.8 to -1.0 V vs. RHE where the second reduction reaction of $[\text{Co-corrole}]^-$ to $[\text{Co-corrole}]^{2-}$ occurs (Fig. 1e).

Characterization of the electrocatalyst on the electrode surface.

Cobalt triphenylphosphine 5,10,15-tris(2,3,5,6-tetrafluoro-4-(MeO-PEG(7))thiophenyl) corrole, $\text{Co}(\text{PPh}_3)_3$ (TpPFC) (-S-PEG(7)-OMe)₃ (“Co-corrole”), is deposited on carbon paper (fabricated via drop casting using a acetonitrile mixture). The catalyst physisorbed on carbon paper was subjected to X-ray photoelectron spectroscopy (XPS) analysis before (Supplementary Table 2) and after the electroreduction (Supplementary Table 3). XPS survey scans exhibited the corresponding Co2p, Co3p, N1s, F1s, S2s, S2p, and P2p binding energy regions (Supplementary Fig. 15). The observed peaks correspond to Co2p, F1s, and P2p in the spectrum of Co-corroles as well as the absence of these peaks in the spectrum of non-modified carbon paper confirmed the

presence of Co-corrole on the carbon paper. The high-resolution Co2p and N1s XP spectra (Supplementary Fig. 15) are in good agreement with previously published XPS data from CoTPP multilayer films^{41,51}.

The main peak for Co $2p_{3/2}$ at 780.18 eV , is located at a typical cobalt(II) position (e.g., 780.2 eV for CoO) and the main peak for N1s is at 398.53 eV . Supplementary Fig. 15 displays also a C1s XP spectrum taken after electrocatalysis reaction. We observe two signals at 284.6 and 286.2 eV , because not all aromatic carbon atoms in the Co-corrole are the same, due to a lowering of symmetry to C_{2v} for corroles relative to D_{4h} for porphyrins. The shake-up satellite at 289.0 eV is typical for organic molecules with extended conjugated π systems. The XPS scans show that the catalyst is stable in course of electrocatalysis (Supplementary Fig. 15).

Heterogeneous CO_2 electroreduction.

The heterogeneous electrochemical CO_2 reduction experiments were carried out with Co-corrole deposited on carbon paper with effective loadings of 0.2 mg cm^{-2} . The modified electrode was found to reduce CO_2 to ethanol and methanol in 0.1 M NaClO_4 at a potential of -0.8 V vs. RHE ($\text{pH} = 6.0$, 0.1 M phosphate buffer, Table 1). Controlled potential electrolysis (CPE) under CO_2 of Co-corrole modified carbon paper exhibits a $\text{TON} = 196$ and a $\text{TOF} = 0.011\text{ s}^{-1}$ for the catalytic conversion of CO_2 to EtOH over 5 h (Fig. 2a–d). The quantification of products was performed using the observed ^1H -nuclear magnetic resonance (NMR)- and gas chromatography mass spectrometry (GC-MS) measurement (e.g., in Fig. 3a and Table 1, and Supplementary Notes 1–3). XPS analysis of the

Table 1 Average Faradaic efficiency for each product detected on the Co-corrrole-carbon paper electrode

Potential V vs. RHE	Faradaic Efficiency of each reduced products on Co-corrrole-carbon paper electrode after 5 h of controlled potential electrolysis at the mentioned potentials ^a							Total FE%	Charge passed (Coulomb)
	CH ₃ CH ₂ OH	CH ₃ OH	HCOO ⁻	CH ₃ COO ⁻	H ₂	HCOH	(CHO) ₂		
	FE%	FE%	FE%	FE%	FE%	FE%	FE%		
-0.515	-	59	12	-	17	10	-	98	35
-0.585	5	52	10	-	22	6	3	98	36
-0.650	10	45	8	1	27	5	2	98	39
-0.700	23	32	6	4	27	5	2	99	40
-0.730	39	23	5	5	20	3	3	98	42
-0.770	44	14	4	8	26	2	1	99	43
-0.800	48	8	1	10	28	1	3	99	44
-0.855	47	5	-	12	33	-	2	99	47
-0.905	45	3	-	12	37	-	1	98	50
-0.955	47	2	-	13	36	-	-	98	53

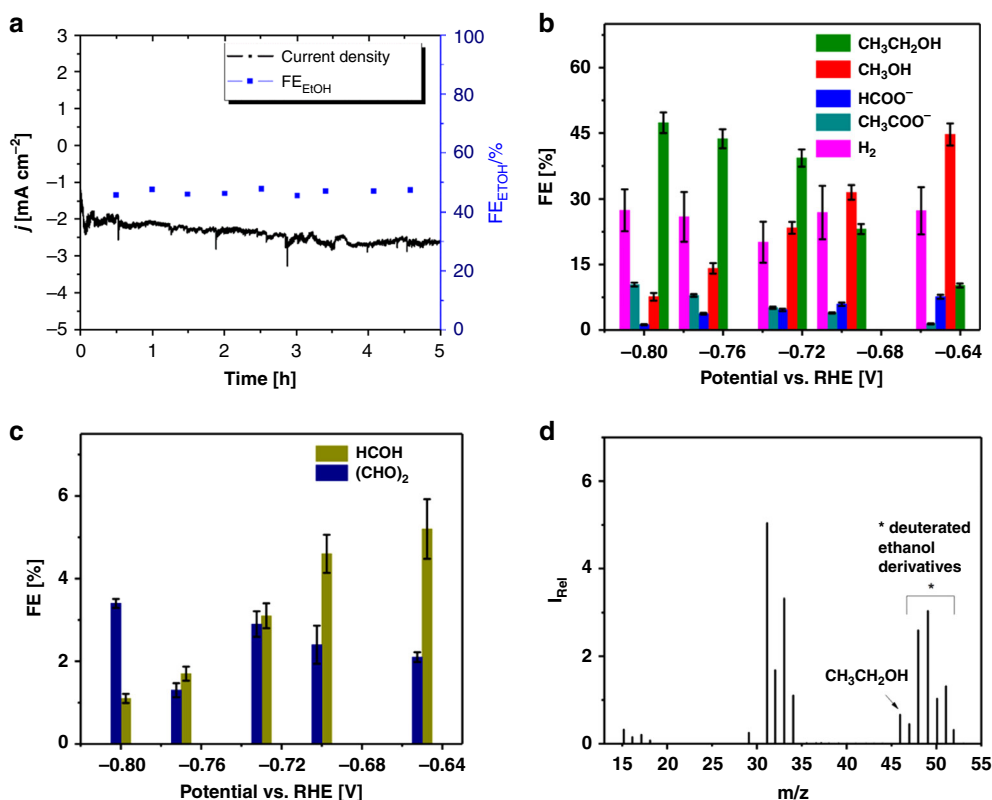
^aIn 0.1 M NaClO₄ (0.1 M pH = 6.0 phosphate buffer)

Fig. 2 **a** Constant potential electrolysis of electrochemical CO₂ reduction by the Co-corrrole modified carbon paper electrode at a potential of -0.8 V vs. RHE (black curve), Faradaic efficiency for ethanol production over 5 h electrolysis (blue rectangles). **b** FE% vs. potential plot for potential dependent product formation. **c** FE% vs. potential plot for minor formed formaldehyde and solvated dimer of formaldehyde at different potentials. The error bars represent standard deviation of six measurements (three electrochemical reactions with two product analysis measurements for each reaction). **d** MS spectra obtained after electrolysis at -0.8 V vs. RHE in (1:3) D₂O/H₂O 0.1 M NaClO₄ saturated with CO₂

electrode materials before and after catalysis reveals that the catalyst is stable in course of electroreduction and the catalyst pertaining to the reduction process are molecular Co-corrrole units (Supplementary Fig. 15). Moreover, in the course of 5 h electrolysis at -0.8 V vs. RHE the Faradaic efficiency (FE%) for the ethanol production was measured at different intervals of time (Fig. 2a). Figure 2a illustrates that the FE = ~48% stays constant throughout the electrocatalytic reduction process.

Subsequently, we have performed CPE with the modified carbon paper electrodes at different potentials, between -0.515 to -0.955 V vs. RHE for 5 h with current densities of 1.9–2.9 mA cm⁻². H₂ is the main gaseous compound and in the liquid phase ethanol, methanol, acetate, formaldehyde, glyoxal, and formate was detected. The quantifications of the respective gaseous and liquid compounds are summarized in Fig. 2b, c, Table 1, and Supplementary Figs. 16–23. During the CO₂ reduction process,

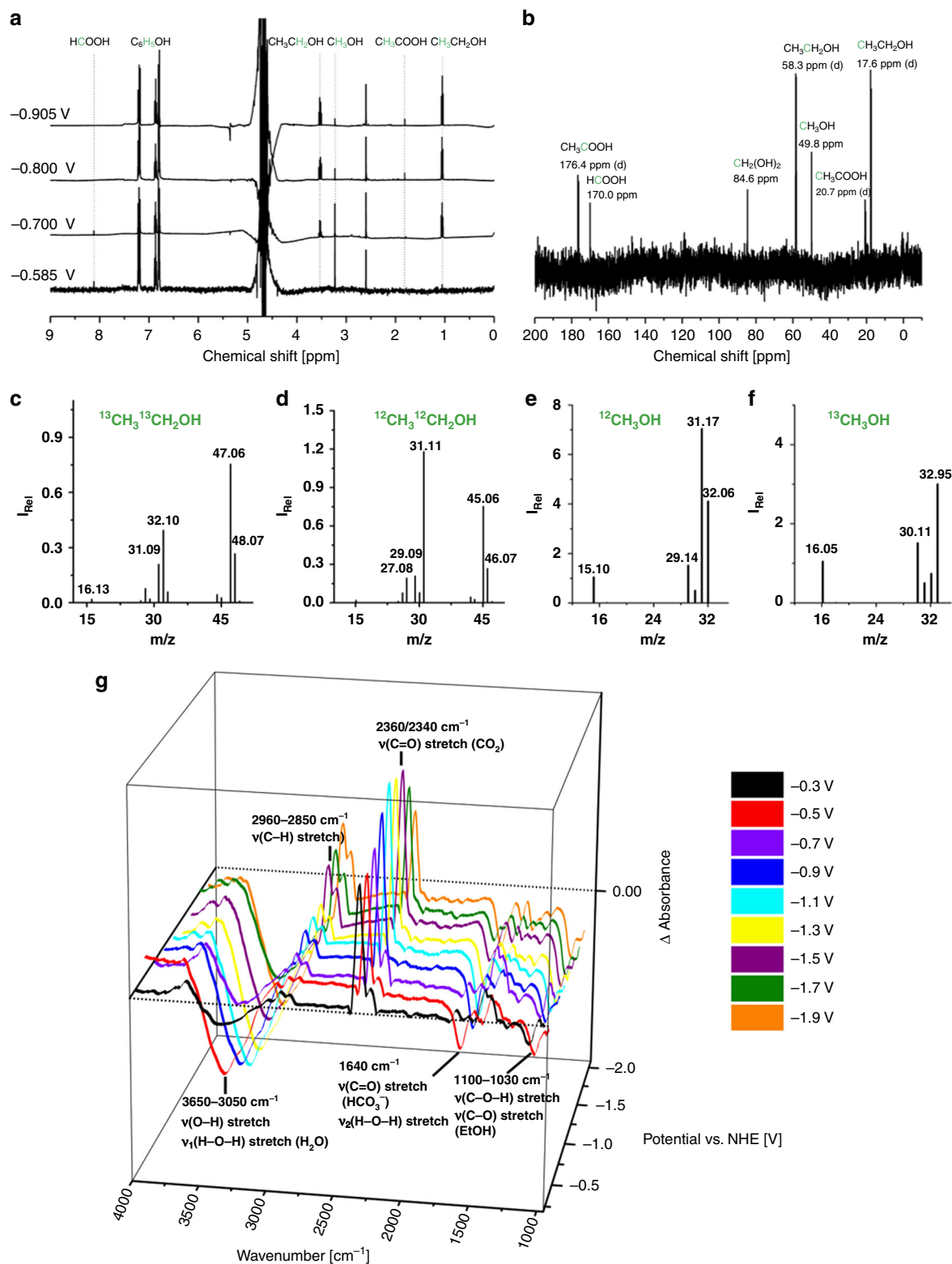


Fig. 3 **a** $^1\text{H-NMR}$ spectrum of the electrolyte after 5 h of CO_2 electrolysis over Co-corrrole-carbon paper electrode at -0.585 , -0.7 , -0.8 , and -0.905 V vs. RHE in 0.1 M NaClO_4 , pH = 6, phosphate buffer, and phenol as the internal standard in DMSO. **b** $^{13}\text{C-NMR}$ (101 MHz, $\text{H}_2\text{O}:\text{D}_2\text{O} = 5:1$) of the electrolyte after 5 h of electrolysis at -0.8 V vs. RHE in $^{13}\text{CO}_2$, 0.1 M NaClO_4 , pH = 6, phosphate buffer. **c-f** GC-MS spectrum of the electrolyte after bulk electrolysis at -0.8 V vs. RHE in $^{12}\text{CO}_2$ and $^{13}\text{CO}_2$: **c** ^{13}C enriched ethanol, **d** ^{12}C enriched ethanol, **e** ^{12}C enriched methanol, and **f** ^{13}C enriched methanol. **g** SEC-FTIR spectra during the CO_2 reduction with 20 mM Co-corrrole in 0.1 M TBAPF_6 (in $\text{CH}_3\text{CN}/\text{H}_2\text{O} = 4:1$), at potentials from -0.3 to -1.9 V vs. NHE

the FE% for ethanol was found in the range of 9–48 with the selectivity for C₂ over C₁ increasing with increase in the applied cathodic potential from –0.73 to –0.96 V vs RHE with a significant decrease in methanol production. CPE long-term measurements were performed at –0.73 V (pH = 6.0) and –0.70 V (pH = 7.2) vs. RHE, where the activity of the Co-corrole modified carbon electrodes retained for 140 h (Supplementary Figs. 8–13).

To further trace the origin of methanol and ethanol, we carried out CO₂ reduction experiments with a D₂O/H₂O mixture. Deuterium distribution during the CO₂ reduction process was monitored by conducting electrolysis at –0.8 V vs. RHE in D₂O/H₂O (1:3). After electrolysis, the mass spectra indicated the formation of reduced product and the following peaks appeared—*m/z* of 45–52 (Fig. 2d). Among the peaks obtained, the one with *m/z* value 52 (CD₃CD₂OD) can be assigned for hexa-deuterated ethanol. In the spectrum apart from the molecular ion peak, there are also peaks corresponding to other fragments with *m/z* = 50 which can be from CD₃CD₂O and *m/z* = 34 for CD₂OD⁺ which are characteristic fragments of CD₃CD₂OD. This deuteration further proves that the source and incorporation of protons in the reduced product is from the solvent and the source of ethanol is from CO₂ reduction. To confirm the source of carbon in the reduction products, we have conducted the reduction experiments with ¹²CO₂ and ¹³CO₂. The ¹H and ¹³C-NMR spectra after CO₂ reduction at the Co-corrole modified carbon paper electrode exhibit resonances for ethanol, methanol, acetic acid, and formic acid (Fig. 3a, b). The ¹³C-NMR spectrum after the reduction of ¹³CO₂ clearly indicates four doublets at 58.3 ppm (¹J_{CC,EtOH} = 37.5 Hz), 17.6 ppm (¹J_{CC,EtOH} = 37.5 Hz), 176.4 ppm (¹J_{CC,acetic acid} = 56.2 Hz), and 20.7 ppm (¹J_{CC,acetic acid} = 56.2 Hz) indicating the reduction of ¹³CO₂ and formation of C–C bond (Fig. 3b). HCOOH and CH₃OH appear as singlets at 170.0 and 49.8 ppm in the ¹³C-NMR spectrum (Fig. 3b), respectively. These results were further substantiated by GC–MS data, which shows a shift of *m/z* = 2 for the molecular ion peak of CH₃CH₂OH⁺ on ¹³C enrichment (Fig. 3c, d). The results for CH₃OH⁺, when compared to ¹²CO₂ reduction shows a shift by *m/z* = 1 (Fig. 3e, f). On analysis of the fragmentation patterns, we observe that for ethanol obtained by the reduction of ¹²CO₂, the peak at *m/z* = 29 corresponds to the CH₃CH₂⁺ ion. On the other hand, when ¹³CO₂ is used, the peak occurs at *m/z* = 31, which is due to the substitution of both ¹²C centers with ¹³C isotopes. Likewise, the peak obtained at *m/z* = 31 in case of ¹²C enriched ethanol resembles the CH₂OH⁺ fragment which on ¹³C enrichment shifts to *m/z* = 32. For ¹²C enriched methanol, the peak at *m/z* = 15 resembles CH₃⁺ ion which shifts to *m/z* = 16 on ¹³C enrichment. The results obtained from both the ¹³C-NMR and GC–MS experiments prove that the source of ethanol as well as methanol is CO₂ (Fig. 3b–f).

Spectroelectrochemical Fourier-transform infrared spectroscopy (FTIR) measurements (SEC-FTIR) at applied potentials of –0.3 to –1.9 V vs. NHE, illustrated in Fig. 3g exhibit increasing IR bands at 3400 cm^{–1} (O–H stretching), 2960 cm^{–1} (C–H stretching), 2850 cm^{–1} (C–H stretching), 1100–1060 cm^{–1} (C–O stretching), indicating the stepwise increase of [alcohol/acid] formation. The IR-band at 1640 cm^{–1} (C = O stretching of HCO₃[–]) indicates the formation of a bicarbonate species. The corresponding IR bands for CO₂ at 2360 and 2340 cm^{–1} (C = O stretching CO₂) decrease during the reaction, indicating that CO₂ is converted under these conditions.

Discussion

An in-depth elucidation of the mechanistic pathway of the reduction process is beyond the scope of this present work. Detailed investigations are underway in our laboratories. To

increase the CO₂ reduction efficiency and to avoid hydrogen evolution at low-pH values, all experiments were performed under weak acidic conditions (pH = 6.0, 0.1 M phosphate buffer). CO₂ reduction under heterogenized conditions with Co-corrole modified carbon electrodes exhibits a redox couple being [Co-corrole]^{1–}/[Co-corrole]^{2–}, which was found to be at –0.8 V vs. RHE. This markedly resembles the redox behavior of the Co-corrole molecule in the solution, so the redox properties are unperturbed upon heterogenization. We thus propose the molecular characteristics of the electrocatalyst to be persistent upon heterogenization. The EPR spectrum obtained after electrochemical reduction and subsequent dosage of CO₂ at room temperature exhibits a rhombic *S* = 1/2 signal at *g* = 2 with a weak ⁵⁹Co hyperfine splitting and indicates the formation of Co(III)–CO₂^{•–} species (Supplementary Fig. 24).

The role of protons is extremely crucial in this work and sets this process apart from related CO₂ reduction processes. For instance, at pH = 6.0 the necessary protons are provided for the subsequent proton coupled electron transfer (PCET), due to this, reduction to methanol/ethanol takes place (Fig. 3a). By performing the same experiment at pH = 7.2, we experimentally observe the reduction of CO₂ to a mixture of formaldehyde, ethanol, methanol, acetate, and formate (see assignment of NMR resonances in the supplementary Fig. 20), and at a pH = 8.0 we detect only CO as the main reduction product (Supplementary Fig. 25a–c and Supplementary Notes 4, 5). This implies that the rate of PCET drastically decreases at weakly to moderately basic pH values. For the successful chemical transformation of CO₂ to methanol and ethanol, this result is crucial in the present context.

The existence of the Co(III)–CO₂^{•–} can only be justified through the presence of CO₂^{•–} formed at a very high potential of *ca.* –1.5 V vs. RHE⁵². But in our case, the reduction wave at *ca.* –0.8 V vs. RHE is responsible for the CO₂ reduction. This implies that the Co(I) in the center of the corrole complex enables the reduction of CO₂ to the CO₂^{•–} intermediate at a lower cost of energy.

We suggest a mechanism similar to that proposed by Koper et al.⁵³ which is illustrated in Fig. 4. The reaction follows a low energy pathway where the carboxyhydroxyl intermediate gets simultaneously reduced by 1 e[–], gets protonated to form a HCO₂H intermediate and can be detected by ¹H-NMR spectroscopy (Fig. 3a, Supplementary Table 4, and Supplementary Notes 6–8). The HCO₂H intermediate further undergoes 1e[–] reduction with the elimination of OH[–] to give HCO[•] stabilized at the Co(III) site. Low potential for reactivity then drives the reaction toward methanol. This reduction pathway of HCO[•] to CH₃O[•] at the cobalt site is in accordance with the mechanism reported by Koper et al. On the other hand, at a higher potential (>–0.73 V vs. RHE) an increased concentration of HCO[•] is developed and, the reaction takes a second route with the recombination of two formyl radicals (Co(III)–HCO[•]+ HCO[•]) leading to oxaldehyde intermediate (OHC–CHO). OHC–CHO was previously reported to be a precursor for the formation of ethanol as well as a key intermediate for C–C step-up leading to C₂ products⁵⁴. The π-conjugation present in OHC–CHO inherently makes it prone to reduction giving [•]OCH₂–CHO which subsequently reduces to [•]OCH₂–CH₂OH which further reduces to CH₃CH₂OH. The high selectivity for alcohol is due to the formation of the HCO[•] intermediate which is readily reducible to methanol. In the case of ethanol, we believe the formation of oxaldehyde intermediate opens up a more favorable route to form ethanol.

The proposed reaction pathways for the formation of the methanol and ethanol were further substantiated by conducting reduction studies of possible intermediates like formic acid, formaldehyde, methanol, and glyoxal under the same reaction conditions reported for Co-corrole–carbon paper electrodes. To

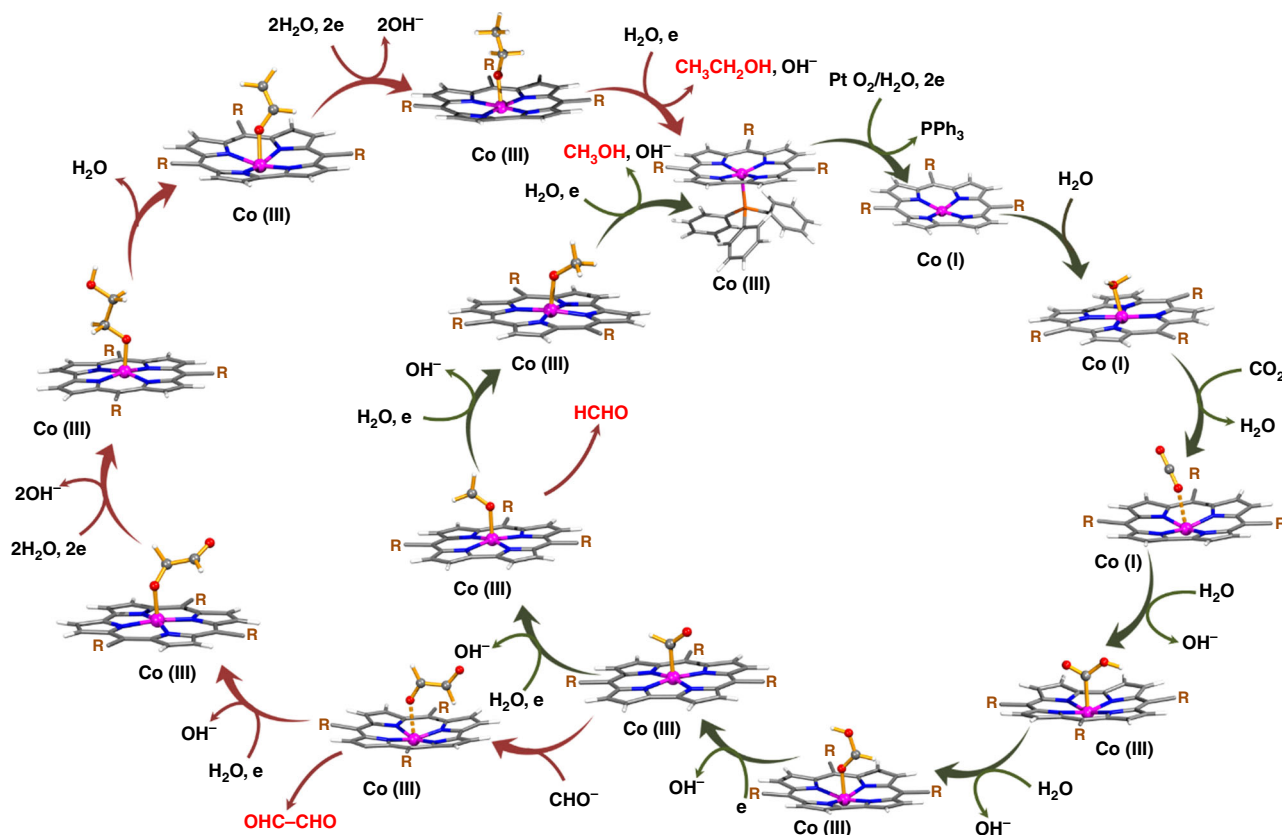


Fig. 4 Proposed single site mechanism of CO₂ reduction using Co-corrole

test this conjecture, further reduction of the 2e⁻ reduced product formic acid was induced, where it yielded a mixture of methanol and ethanol which indeed implies formic acid to be an important intermediate. Cyclic voltammetric measurements show an increase in current density (Supplementary Fig. 34a) upon the addition of 10 mM of formic acid. CPE was performed at -0.73 V vs. RHE over Co-corrole-carbon paper for 5 h and the products obtained were analyzed in GC-MS spectrum where the presence of the characteristic peaks of methanol (*m/z* = 32) and ethanol (*m/z* = 46) were observed (Supplementary Figs. 36–38). The obtained results were further confirmed by ¹H-NMR spectroscopy (Supplementary Fig. 34b). The proposed HCOOH intermediate under the low potential of reactivity gets reduced to HCHO and methanol, which are the final products and does not get further reduced. To verify the role of oxaldehyde in the current mechanistic cycle, 0.1 mM OHC-CHO was externally added under the reaction condition and CH₃CH₂OH was obtained proving oxaldehyde to be a key intermediate for CH₃CH₂OH formation (Supplementary Fig. 35a, b). The high selectivity for alcohol is primarily due to the formation of the formic acid intermediate followed by formation of HCO[•] intermediate which is readily reducible to methanol. In the case of ethanol, we believe the formation of oxaldehyde is due to coupling of two HCO[•] intermediate which opens up a more favorable route to form ethanol. To complete the studies, we performed comparative measurements with two similar Co-corroles (cobalt triphenylphosphine 5,10,15-tris(pentafluoro-phenyl) corrole (PPh₃-CoTpPFC) and cobalt triphenylphosphine 5,10,15-triphenyl corrole PPh₃-CoTPC)), which consist of (a) three *meso*-C₆F₅-groups or of (b) three *meso*-C₆H₅-groups. The results are illustrated in the Supplementary Informations file of the paper (Supplementary Fig. 43). The main reduction products under the same reaction conditions at pH = 6 were assigned to formic acid,

methanol, and acetic acid. Only trace amounts of ethanol were found employing these two catalyst systems.

To conclude, we have demonstrated the electrochemical reduction of CO₂ to ethanol and methanol with a Co-corrole-carbon paper electrode at a low potential (-0.8 V vs. RHE) with a FE of 48% over a time period of 5 h. The Co-corrole-carbon paper electrode can withstand extremely high operational time of up to 140 h marking the highest efficiency for a molecular electrocatalyst reported so far in the literature. This is accomplished by the formation of a OHC-CHO type intermediate using a MeO-PEG(7)-S-modified cobalt corrole molecular catalyst. The Co-corrole molecule tends to stabilize different radical intermediates at the metal site. Thus, when reacted with a greater number of electrons highly reduced products are formed. On simulating the reactivity of Co-corrole, we found both experimentally and theoretically that in contrast to the CO pathway our catalyst proceeds via a formic acid pathway. By applying a redox potential of -0.73 V vs. RHE, a mixture of methanol and ethanol is detected. The obtained reaction products can only be explained if formic acid is developed temporarily, which is subsequently reduced to the formyl radical (HCO[•]). The HCO[•] forms methanol as well as glyoxal and ultimately the glyoxal is then reduced to form ethanol serving our catalyst to operate at a low over potential.

Methods

Chemicals. All chemicals and solvents were commercially available and were used as obtained, unless otherwise noted. High-performance liquid chromatography grade solvents were used in all the experiments with water, methanol, acetonitrile, and sodium perchlorate (NaClO₄) purchased from Merck, tetrabutylammonium perchlorate (Bu₄NClO₄), and Ferrocene from Sigma Aldrich. Tetrabutylammonium hexafluorophosphate (Bu₄NPF₆), 98%, purchased from Alfa Aesar, was twice recrystallized with absolute Ethanol, dried under high vacuum and stored under nitrogen. The 5,10,15-trispentafluorophenylcorrole was synthesized

according to the Gryko's method for highly reactive aldehydes⁴⁸. For NMR experiments D₂O was purchased from Cambridge Isotopic Laboratory. GC authentic standard ethanol, methanol, glyoxal, and diethoxymethane were purchased from Sigma Aldrich. Toray Carbon Paper, TGP-H-60, 19 × 19 cm was purchased from Alfa Aesar. 2,2,6,6-tetramethyl-1-piperidinyloxy, free radical, 2,2,6,6-tetramethylpiperidine 1-oxyl, TEMPO was purchased from Sigma Aldrich. ¹³CO₂ (99.0 atom%) from Icon isotopes USA and Sigma Aldrich. CO₂ and Ar used in the electrochemical measurements were purchased from Praxair with a purity of 99.995%.

Materials synthesis and characterization

Free base 5,10,15-tris(2,3,5,6-tetrafluoro-4-(MeO-PEG(7))thiophenyl)corrole H₃TpFPC (-S-PEG(7)-OMe)₃. 250 mg 5,10,15-tris(pentafluorophenyl)corrole (H₃TpFPC) (314 μmol) and 225 mg sodium hydride (60% in mineral oil, 30 equiv., 9.4 mmol) were given in a 250 mL two-neck round-bottom flask under argon atmosphere. Totally, 100 mL THF_{abs.} and 336 mg MeO-PEG(7)-thiol (3 equiv., 942 μmol) were added and the reaction was stirred at room temperature for 30 min. The reaction was controlled via TLC and mass spectroscopy. To quench the reaction, 15 mL H₂O_{dest.} were added. Further saturated aqueous NH₄Cl-solution was added and the solution was extracted three times with ethylacetate. The combined organic phases were washed with 0.1 M HCl, dried over Na₂SO₄, filtered and evaporated to dryness. The product H₃TpFPC(-S-PEG(7)-OMe)₃ (517.8 mg, 0.267 mmol, 91.3 %) was obtained as a turquoise solid.

¹H-NMR (300.1 MHz, CDCl₃, 25 °C): δ = 9.09 (2H, d, ³J = 4.14 Hz, H2 + H18), 8.80 (2H, d, ³J = 4.38 Hz, H7 + H13), 8.61–8.58 (4H, m, H8 + H12 + H3 + H17), 3.91 (6H, t, ³J = 6.20 Hz, -CH₂), 3.74–3.71 (12H, m, -CH₂), 3.68–3.65 (12H, m, -CH₂), 3.61 (12H, bs, -CH₂), 3.56–3.55 (18H, m, -CH₂), 3.52–3.49 (6H, m, -CH₂), 3.42–3.39 (12H, m, -CH₂), 3.26 (9H, s, -CH₃) ppm (Supplementary Fig. 1).

¹⁹F-NMR (282.4 MHz, CDCl₃, 25 °C): δ = -133.63 (4F, dd, ³J = 25.20 Hz, ⁴J = 11.87 Hz, Fo), -134.06 (2F, dd, ³J = 25.76 Hz, ⁴J = 12.12 Hz, Fo), -137.56 (2F, dd, ³J = 25.50 Hz, ⁴J = 12.21 Hz, Fm), -138.22 (4F, dd, ³J = 24.94 Hz, ⁴J = 11.73 Hz, Fm) ppm (Supplementary Fig. 2).

HRMS (ESI, positive): *m/z* calculated for C₈₂H₁₀₄F₁₂N₄O₂₁S₃: 1805.6236 [M+H]⁺, 1827.6061 [M+Na]⁺; found: 1805.6273 [M+H]⁺, 1827.6096 [M+Na]⁺ (Supplementary Fig. 3).

Co-Corrole: Co(PPh₃)(TpFPC)(-S-PEG(7)-OMe)₃. Totally, 385.2 mg of H₃TpFPC (-S-PEG(7)-OMe)₃ (0.213 mmol) were dissolved in 250 mL DCM: MeOH (2:1) in a 250 mL two-neck round-bottom flask under argon atmosphere. Cobalt(II)acetate tetrahydrate (539.7 mg, 2167 μmol, 10 equiv.) and triphenylphosphine (58.5 mg, 0.233 mmol, 1 equiv.) were added and the reaction mixture was heated to reflux for an hour. The reaction progress was monitored via UV/vis and TLC. After complete metalation, the mixture was extracted with DCM. The combined organic phases were extracted four times with water, dried over Na₂SO₄, filtered and evaporated under reduced pressure. Purification was performed with silica gel column chromatography (DCM/MeOH = 20:1), where the red product Co(PPh₃)(TpFPC)(-S-PEG(7)-OMe)₃ was obtained with 54.4% yield (246.3 mg, 115.9 μmol).

¹H-NMR (300.1 MHz, CDCl₃, 25 °C): δ = 8.68 (2H, d, ³J = 4.50 Hz, H2 + H18), 8.36 (2H, d, ³J = 4.77 Hz, H7 + H13), 8.26 (2H, d, ³J = 4.74 Hz, H8 + H12), 8.12 (2H, d, ³J = 4.47 Hz, H3 + H17), 7.04–6.99 (3H, m, triphenylphosphine-CH), 6.69–6.64 (6H, m, triphenylphosphine-CH), 4.64–4.58 (6H, m, triphenylphosphine-CH), 3.91–3.86 (6H, m, -CH₂), 3.74–3.69 (24H, m, -CH₂), 3.65–3.59 (42H, m, -CH₂), 3.52–3.49 (6H, m, -CH₂), 3.35 (9H, s, -CH₃) ppm (Supplementary Fig. 4).

¹⁹F-NMR (282.4 MHz, CDCl₃, 25 °C): δ = -133.88 to -133.72 (3F, m, Fo), -134.47 to -134.21 (3F, m, Fo), -136.99 (3F, dd, ³J = 25.47 Hz, ⁴J = 12.00 Hz, Fm), -137.30 (1F, dd, ³J = 25.44 Hz, ⁴J = 12.10 Hz, Fm), -138.08 (3F, dd, ³J = 25.81 Hz, ⁴J = 11.94 Hz, Fm), -138.44 (1F, dd, ³J = 25.80 Hz, ⁴J = 12.09 Hz, Fm) ppm (Supplementary Fig. 5).

HRMS (APPI, positive): *m/z* calculated for C₈₂H₁₀₄F₁₂N₄O₂₁S₃: 2145.6064 [M+Na]⁺; found: 2145.6078 [M+Na]⁺ (Supplementary Fig. 6).

Preparation of the working electrode. The working electrode consists of cobalt (III)-corrole immobilized over carbon fiber paper (A = 1 cm²). For this, a 0.5 mL solution of cobalt(III)-corrole in acetonitrile was prepared and drop-casted over carbon fiber to make a loading of 0.2 mg cm⁻². Further, we preserve the electrodes at room temperature to remove the excess acetonitrile. Then these electrodes were washed with 0.1 M pH = 6 phosphate buffer to get rid of the acetonitrile completely. Then the electrodes were dried in presence of CaCl₂ under high vacuum.

Cyclic voltammetry and CPE. Cyclic Voltammetry and CPE for CO₂ reduction were performed with a workstation (CH Instruments, Model CHI400A) in a two-compartment, three-electrode electrochemical H-cell, consisting of a gas tight cell with a total volume of 30 mL. Carbon paper was used as the working electrode. Ag/AgCl (*E*_{Ag/AgCl} = 0.222 V filled with 0.1 M KCl) as the reference, and Pt wire as the counter. The reference electrode potential was calibrated with respect to the reversible hydrogen potential using platinum working electrode and platinum wire as counter electrode in 0.5 M H₂SO₄ electrolyte in H₂ atmosphere. This calibration result showed a shift of -0.222 V versus the NHE. All experiments were carried out

at 25 °C. The pH value of the solutions were obtained using a EUTECH pH 510 pre-calibrated with Thermo Scientific pH 4.01, 7.0, and 10.01 buffer solutions. For all the measurements CO₂ was continuously purged into the solution. All the potentials are represented in RHE scale with iR correction.

For electrochemistry in non-aqueous medium, acetonitrile was used as the solvent of choice with a similar electrochemical setup with glassy carbon as the working electrode, Ag/AgCl (0.1 M KCl) as the reference and Pt wire as the counter electrode with 0.1 M tetrabutylammonium perchlorate or 0.1 M tetrabutylammonium hexafluorophosphate as the electrolyte. Under this electrochemical conditions, the redox behavior of 0.01 M ferrocene in acetonitrile was studied, which was further used as the internal standard.

Detection and quantification of the CO₂ reduced products. ¹H- and ¹³C-NMR spectroscopy of the carbon dioxide reduced liquid products were recorded on a Bruker Ascend 700 MHz Avance III NMR spectrometer equipped with a cryoprobe and on a JEOL ECS-400 NMR spectrometer. As internal standard, 20 mL aqueous solution of 20 mM phenol and 10 mM of dimethyl sulfoxide were used. After CPE, to 350 μL electrolyte, 200 μL D₂O, and 50 μL of the internal standard were added and transferred into a NMR-tube. During the measurements, the water peak was suppressed to increase the signal intensity of the analytes. The CO₂ reduced products were further analyzed using GC-MS. Trace 1300 GC and ISQ QD single quadrupole GC-MS instrument with a TG-5MS capillary column (30 m × 0.32 mm × 0.25 μm) supplied by Thermo Fisher Scientific and DB-624 capillary column (30 m × 0.32 mm × 0.25 μm) supplied by Agilent were used for the same. For gaseous analysis CarboPLOT 007 capillary column (25 m × 0.53 mm × 0.25 μm) supplied by Agilent was used for separation and TCD for detection.

Electrochemically active surface area (ECSA) calculation. ECSA value is obtained by using the following equation

$$ECSA = C_D / C_S \quad (1)$$

where *C_D* = electrochemical double layer capacitance which is obtained from the slope of the current vs. scan rate plot in the non-Faradaic region and *C_S* = specific capacitance of the sample and in this case, *C_S* = 0.040 mF cm⁻²⁵⁵.

Analysis of the CO₂ reduced products in ¹H-NMR and GC-MS. Compounds formed at different potentials were detected directly by ¹H-NMR (integrated with respect to DMSO (δ = 2.71 ppm) as an internal standard) with a triplet signal at δ = 1.17 ppm and a quartet at δ = 3.67 ppm indicating ethanol (Supplementary Fig. 17); a singlet at δ = 3.37 ppm showing the presence of methanol (Supplementary Fig. 17).

For detection of formaldehyde, 2 mL of the reaction mixture was taken in a 20 mL headspace vial with 25 μL of ethanol and was acidified with 100 μL 1% *p*-toluenesulfonic acid. This mixture was then heated at 60 °C for 1 h and then GC-MS measurements were done⁵⁶. In the mass spectrum, peak centered at *m/z* = 104 represents diethoxymethane indicating the formation of formaldehyde with a retention time around 3.00 min (Supplementary Figs. 39 and 40). Glyoxal was detected in the spectrum at *m/z* = 58 with a retention time of 3.35 min (Supplementary Figs. 41 and 42).

XPS measurements. XPS was performed by using a Theta Probe, ThermoFisher, UK, using monochromatic Al Kα X-rays (*hν* = 1486.6 eV), spot size 400 microns and with a photoelectron take-off angle of 90° with respect to the surface plane. The binding energies were corrected using the C1s peak at BE = 284.6 eV that arises from adventitious hydrocarbon.

Data availability

The data that support the findings of this study are available from the corresponding authors upon reasonable request.

Received: 3 December 2018 Accepted: 8 August 2019

Published online: 27 August 2019

References

1. Enthaler, S., Langermann, Jvon & Schmidt, T. Carbon dioxide and formic acid —the couple for environmental-friendly hydrogen storage? *Energy Environ. Sci.* **3**, 1207–1217 (2010).
2. Kondratenko, E. V., Mul, G., Baltrusaitis, J., Larrazábal, G. O. & Pérez-Ramírez, J. Status and perspectives of CO₂ conversion into fuels and chemicals by catalytic, photocatalytic and electrocatalytic processes. *Energy Environ. Sci.* **6**, 3112–3135 (2013).
3. Piontek, S. et al. Bio-inspired design: bulk iron–nickel sulfide allows for efficient solvent-dependent CO₂ reduction. *Chem. Sci.* **10**, 1075–1081 (2019).
4. Albo, J. et al. Copper-based metal-organic porous materials for CO₂ electrocatalytic reduction to alcohols. *ChemSusChem* **10**, 1100–1109 (2017).

- Roy, S. et al. Molecular cobalt complexes with pendant amines for selective electrocatalytic reduction of carbon dioxide to formic acid. *J. Am. Chem. Soc.* **139**, 3685–3696 (2017).
- Seh, Z. W. et al. Combining theory and experiment in electrocatalysis. Insights into materials design. *Science* **355**, eaad4998 (2017).
- Aresta, M., Dibenedetto, A. & Angelini, A. Catalysis for the valorization of exhaust carbon. from CO₂ to chemicals, materials, and fuels. Technological use of CO₂. *Chem. Rev.* **114**, 1709–1742 (2013).
- Lantern, A. E. & Scaiano, J. C. Photoinduced hydrogen fuel production and water decontamination technologies. Orthogonal strategies with a parallel future? *ACS Energy Lett.* **2**, 1909–1910 (2017).
- Han, N. et al. Ultrathin bismuth nanosheets from in situ topotactic transformation for selective electrocatalytic CO₂ reduction to formate. *Nat. Commun.* **9**, 1320 (2018).
- Liu, Y. et al. Selective electrochemical reduction of carbon dioxide to ethanol on a boron- and nitrogen-Co-doped nanodiamond. *Angew. Chem. Int. Ed.* **56**, 15607–15611 (2017).
- Lacy, D. C., McCrory, C. C. L. & Peters, J. C. Studies of cobalt-mediated electrocatalytic CO₂ reduction using a redox-active ligand. *Inorg. Chem.* **53**, 4980–4988 (2014).
- Grodzowski, J. et al. Reduction of cobalt and iron corroles and catalyzed reduction of CO₂. *J. Phys. Chem. A* **106**, 4772–4778 (2002).
- Fisher, B. J. & Eisenberg, R. Electrocatalytic reduction of carbon dioxide by using macrocycles of nickel and cobalt. *J. Am. Chem. Soc.* **102**, 7361–7363 (1980).
- Beley, M., Collin, J.-P., Ruppert, R. & Sauvage, J.-P. Nickel (II)-cyclam. An extremely selective electrocatalyst for reduction of CO₂ in water. *Chem. Commun.* **135**, 1315–1316 (1984).
- Hawecker, J., Lehn, J.-M. & Ziessel, R. Electrocatalytic reduction of carbon dioxide mediated by Re (bipy)(CO)₃Cl (bipy = 2, 2'-bipyridine). *Chem. Commun.* **6**, 328–330 (1984).
- Cosnier, S., Deronzier, A. & Moutet, J.-C. Electrocatalytic reduction of CO₂ on electrodes modified by fac-Re(2,2'-bipyridine)(CO)₃Cl complexes bonded to polypyrrole films. *J. Mol. Catal.* **45**, 381–391 (1988).
- Cabrera, C. R. & Abuña, H. D. Electrocatalysis of CO₂ reduction at surface modified metallic and semiconducting electrodes. *J. Electroanal. Chem. Interfacial Electrochem.* **209**, 101–107 (1986).
- Ren, D., Fong, J. & Yeo, B. S. The effects of currents and potentials on the selectivities of copper toward carbon dioxide electroreduction. *Nat. Commun.* **9**, 925 (2018).
- Kim, D., Resasco, J., Yu, Y., Asiri, A. M. & Yang, P. Synergistic geometric and electronic effects for electrochemical reduction of carbon dioxide using gold-copper bimetallic nanoparticles. *Nat. Commun.* **5**, 4948 (2014).
- Peterson, A. A., Abild-Pedersen, F., Studt, F., Rossmeisl, J. & Nørskov, J. K. How copper catalyzes the electroreduction of carbon dioxide into hydrocarbon fuels. *Energy Environ. Sci.* **3**, 1311–1315 (2010).
- Kas, R. et al. Electrochemical CO₂ reduction on Cu₂O-derived copper nanoparticles. controlling the catalytic selectivity of hydrocarbons. *Phys. Chem. Chem. Phys.* **16**, 12194–12201 (2014).
- Rosen, B. A. et al. Ionic liquid-mediated selective conversion of CO₂ to CO at low overpotentials. *Science* **334**, 643–644 (2011).
- Kuhl, K. P., Cave, E. R., Abram, D. N. & Jaramillo, T. F. New insights into the electrochemical reduction of carbon dioxide on metallic copper surfaces. *Energy Environ. Sci.* **5**, 7050–7059 (2012).
- Wang, Z., Yang, G., Zhang, Z., Jin, M. & Yin, Y. Selectivity on etching. Creation of high-energy facets on copper nanocrystals for CO₂ electrochemical reduction. *ACS Nano* **10**, 4559–4564 (2016).
- Gao, D. et al. Enhancing CO₂ electroreduction with the metal-oxide interface. *J. Am. Chem. Soc.* **139**, 5652–5655 (2017).
- Ma, S. et al. Electroreduction of Carbon Dioxide to Hydrocarbons Using Bimetallic Cu-Pd Catalysts with Different Mixing Patterns. *J. Am. Chem. Soc.* **139**, 47–50 (2017).
- Choi, S. Y., Jeong, S. K., Kim, H. J., Baek, I.-H. & Park, K. T. Electrochemical reduction of carbon dioxide to formate on tin-lead alloys. *ACS Sustain. Chem. Eng.* **4**, 1311–1318 (2016).
- Yuan, J. et al. Electroreduction of CO₂ into ethanol over an active catalyst. Copper supported on titania. *Catalysts* **7**, 220 (2017).
- Hahn, C. et al. Engineering Cu surfaces for the electrocatalytic conversion of CO₂. Controlling selectivity toward oxygenates and hydrocarbons. *Proc. Natl. Acad. Sci. USA* **114**, 5918–5923 (2017).
- Cope, J. D. et al. Electrocatalytic reduction of CO₂ with CCC-NHC pincer nickel complexes. *Chem. Commun.* **53**, 9442–9445 (2017).
- Cook, T. D. et al. Nickel complexes of C-substituted cyclams and their activity for CO₂ and H⁺ reduction. *ACS Omega* **2**, 3966–3976 (2017).
- Huan, T. N. et al. Electrochemical reduction of CO₂ catalyzed by Fe-NC materials. A structure-selectivity study. *ACS Catal.* **7**, 1520–1525 (2017).
- Wu, J. et al. A metal-free electrocatalyst for carbon dioxide reduction to multi-carbon hydrocarbons and oxygenates. *Nat. Commun.* **7**, 13869 (2016).
- Kim, D., Kley, C. S., Li, Y. & Yang, P. Copper nanoparticle ensembles for selective electroreduction of CO₂ to C₂-C₃ products. *Proc. Natl. Acad. Sci. USA* **114**, 10560–10565 (2017).
- Louidice, A. et al. Tailoring copper nanocrystals towards C₂ products in electrochemical CO₂ reduction. *Angew. Chem. Int. Ed.* **55**, 5789–5792 (2016).
- Ren, D., Ang, B. S.-H. & Yeo, B. S. Tuning the selectivity of carbon dioxide electroreduction toward ethanol on oxide-derived Cu x Zn catalysts. *ACS Catal.* **6**, 8239–8247 (2016).
- Hoang, T. T. H. et al. Nano porous copper-silver alloys by additive-controlled electro-deposition for the selective electroreduction of CO₂ to ethylene and ethanol. *J. Am. Chem. Soc.* **140**, 5791–5797 (2018).
- Ren, D. et al. Selective electrochemical reduction of carbon dioxide to ethylene and ethanol on copper(I)oxide catalysts. *ACS Catal.* **5**, 2814–2821 (2015).
- Handoko, A. D. et al. Mechanistic insights into the selective electroreduction of carbon dioxide to ethylene on Cu₂O-derived copper catalysts. *J. Phys. Chem. C* **120**, 20058–20067 (2016).
- Hu, X. M., Rønne, M. H., Pedersen, S. U., Skrydstrup, T. & Daasbjerg, K. Enhanced catalytic activity of cobalt porphyrin in CO₂ electroreduction upon immobilization on carbon materials. *Angew. Chem. Int. Ed.* **56**, 6468–6472 (2017).
- Zhang, X. et al. Highly selective and active CO₂ reduction electrocatalysts based on cobalt phthalocyanine/carbon nanotube hybrid structures. *Nat. Commun.* **8**, 14675 (2017).
- Shen, J. et al. Electrocatalytic reduction of carbon dioxide to carbon monoxide and methane at an immobilized cobalt protoporphyrin. *Nat. Commun.* **6**, 8177 (2015).
- Behar, D. et al. Cobalt porphyrin catalyzed reduction of CO₂. Radiation chemical, photochemical, and electrochemical studies. *J. Phys. Chem. A* **102**, 2870–2877 (1998).
- Kortlever, R., Shen, J., Schouten, K. J. P., Calle-Vallejo, F. & Koper, M. T. M. Catalysts and reaction pathways for the electrochemical reduction of carbon dioxide. *J. Phys. Chem. Lett.* **6**, 4073–4082 (2015).
- Faschinger, F., Aichhorn, S., Himmelsbach, M. & Schoefberger, W. Bismuth A₃-Corroles: useful precursors for the development of meso-substituted free-base corroles. *Synthesis* **46**, 3085–3096 (2014).
- König, M., Faschinger, F., Reith, L. M. & Schöfberger, W. The evolution of corrole synthesis—from simple one-pot strategies to sophisticated ABC-corroles. *J. Porphyr. Phthalocyanines* **20**, 96–107 (2016).
- Schöfberger, W. et al. A bifunctional electrocatalyst for oxygen evolution and oxygen reduction reactions in water. *Angew. Chem. Int. Ed.* **55**, 2350–2355 (2016).
- Gryko, D. T. & Koszarna, B. Refined methods for the synthesis of meso-substituted A₃- and trans-A₂B-corroles. *Org. Biomol. Chem.* **1**, 350–357 (2003).
- Lei, H. et al. Noncovalent immobilization of a pyrene-modified cobalt corrole on carbon supports for enhanced electrocatalytic oxygen reduction and oxygen evolution in aqueous solutions. *ACS Catal.* **6**, 6429–6437 (2016).
- Kadish, K. M. et al. Electrochemistry of rhodium and cobalt corroles. Characterization of (OMC)Rh(PPh₃) and (OMC)Co(PPh₃) where OMC is the trianion of 2,3,7,8,12,13,17,18-octamethylcorrole. *Inorg. Chem.* **31**, 2305–2313 (1992).
- Lukasczyk, T. et al. Interaction of cobalt (II) tetraarylporphyrins with a Ag (111) surface studied with photoelectron spectroscopy. *J. Phys. Chem. C* **111**, 3090–3098 (2007).
- Finn, C., Schnittger, S., Yellowlees, L. J. & Love, J. B. Molecular approaches to the electrochemical reduction of carbon dioxide. *Chem. Commun.* **48**, 1392–1399 (2012).
- Shen, J., Kolb, M. J., Göttle, A. J. & Koper, M. T. M. DFT study on the mechanism of the electrochemical reduction of CO₂ catalyzed by cobalt porphyrins. *J. Phys. Chem. C* **120**, 15714–15721 (2016).
- Schouten, K. J. P., Kwon, Y., van der Ham, C. J. M., Qin, Z. & Koper, M. T. M. A new mechanism for the selectivity to C 1 and C 2 species in the electrochemical reduction of carbon dioxide on copper electrodes. *Chem. Sci.* **2**, 1902–1909 (2011).
- McCrory, C. C. L., Jung, S., Peters, J. C. & Jaramillo, T. F. Benchmarking heterogeneous electrocatalysts for the oxygen evolution reaction. *J. Am. Chem. Soc.* **135**, 16977–16987 (2013).
- del Barrio, M.-A., Hu, J., Zhou, P. & Cauchon, N. Simultaneous determination of formic acid and formaldehyde in pharmaceutical excipients using headspace GC/MS. *J. Pharm. Biomed. Anal.* **41**, 738–743 (2006).

Acknowledgements

W.S. and S.G. acknowledges the financial support of the Austrian Science Fund (FWF-P28167-N34 and FWF-P32045-NBL). S.P. and S.B. acknowledge UGC for fellowships, S.S.S. thanks SERB (PDF/2017/000676), S.R. acknowledges the start-up and FIRE and PRIS grants from IISER Kolkata, India. S.R. further thanks CCNU, P.R. China and NSFC (B050704), P.R. China and '111 project' for financial support. The NMR spectrometers were acquired in collaboration with the University of South Bohemia (CZ) with financial support from the European Union through the EFRE INTERREG IV ETC-AT-CZ.

program (project M00146, “RERI-uasb”). W.S. and S.G. thanks Dr. Markus Himmelsbach for the ESI-MS measurement. P.G. thanks the Fonds of the Chemical Industry for a PhD fellowship. U.-P.A. is grateful for support by the Deutsche Forschungsgemeinschaft (Emmy Noether grant, AP242/2-1; AP242/6-1) and the Fraunhofer Internal Programs under Grant no. Attract 097-602175. U.-P.A. and P.G. were funded by the Deutsche Forschungsgemeinschaft (DFG, German Research Foundation—Germany’s Excellence Strategy, EXC-2033—Project number 390677874).

Author contributions

W.S. and S.R. conceived the project and wrote the paper. W.S., S.G., F.P. and M.H. developed and carried out the syntheses of metal corroles, analytics, and optical characterization. S.P., S.G. and R.D. conducted all electrochemical measurements, experiments with CO₂ reduction, and GC-MS characterizations. W.S., S.G. and S.B. carried out the NMR experiments. S.S.S. did modeling and calculations. U.-P. A. and P.G. performed the SEC-FTIR experiments and the analysis of gaseous products after heterogeneous catalysis. A.A., H.C. and P.S. performed additional long-time electrochemical measurements. S.M. performed the ESR measurements. W.S. and S.R. supervised and coordinated the work. All authors have given approval for the final version of this paper.

Additional information

Supplementary Information accompanies this paper at <https://doi.org/10.1038/s41467-019-11868-5>.

Competing interests: The authors declare no competing interests.

Reprints and permission information is available online at <http://npg.nature.com/reprintsandpermissions/>

Peer review information: *Nature Communications* thanks the anonymous reviewer(s) for their contribution to the peer review of this work.

Publisher’s note: Springer Nature remains neutral with regard to jurisdictional claims in published maps and institutional affiliations.



Open Access This article is licensed under a Creative Commons Attribution 4.0 International License, which permits use, sharing, adaptation, distribution and reproduction in any medium or format, as long as you give appropriate credit to the original author(s) and the source, provide a link to the Creative Commons license, and indicate if changes were made. The images or other third party material in this article are included in the article’s Creative Commons license, unless indicated otherwise in a credit line to the material. If material is not included in the article’s Creative Commons license and your intended use is not permitted by statutory regulation or exceeds the permitted use, you will need to obtain permission directly from the copyright holder. To view a copy of this license, visit <http://creativecommons.org/licenses/by/4.0/>.

© The Author(s) 2019